I&EC research
Industrial & Engineering Chemistry Research
pubs.acs.org/IECR
Article

Unveiled Understanding on Thermodynamic Mechanisms of Atomic Layer Deposition Based on Trimethylaluminum and Water Precursors

Jae Won Choi, So-Yeon Ham, Suhyun Lee, Da-Som Shin, Yo-Sep Min,* and Ki Chul Kim*

Cite This: *Ind. Eng. Chem. Res.* 2020, 59, 13325−13332
Read Online

ABSTRACT: Despite the importance of the atomic layer deposition (ALD) technique for developing thin films of various inorganic materials with the precisely controlled thickness, the detailed mechanistic pathway and thermodynamics of the ALD processes are not fully understood. In this study, the first-principles density functional theory calculations for ALD of Al_2O_3 are employed to explore the reaction thermodynamics in the chemical adsorption of trimethylaluminum (TMA) and water during the TMA- and H_2O-dosed half-cycles of ALD. Three primary conclusions are highlighted from this investigation. (i) Despite the intrinsic nature of the TMA molecule with higher thermodynamic stability in a dimeric form than in a monomeric form, the TMA molecules would prefer to be chemisorbed on $Al_2O_3(0001)$ surfaces in a monomeric form during the TMA-dosed half-cycle, exhibiting the highest stability for the monomeric TMA adsorbates in bidentate configurations under the assumption of the presence of abundant hydroxyl adsorption sites. (ii) The energy profile for the chemisorption of water molecules during the H_2O-dosed half-cycle would strongly rely on the configuration of the TMA adsorbates formed in the previous TMA-dosed half-cycle, especially at the early stage of the H_2O-dosed half-cycle. (iii) The thermodynamic feasibility of the water molecules chemisorbed after the early stage of the H_2O-dosed half-cycle would not be significantly varied in real ALD processes.

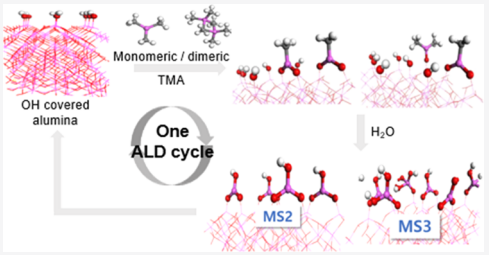

INTRODUCTION

Atomic layer deposition (ALD) has been a popular technique for efficiently depositing thin films of various materials with precise growth control for a variety of applications, such as semiconductor devices, lithium-ion batteries, fuel cells, and solar cells.[1,2] For instance, in semiconductor industries, the thin film deposition with atomic precision is required for miniaturization of the electronic chips.[3−5] Kessels *et al.* reviewed the potential of the ALD technique for developing (ultra)thin films for lithium-ion batteries, fuel cells, and solar cells.[6] Specifically, Scott *et al.* employed the ALD approach to deposit ultrathin protective films on $LiCoO_2$ cathode particles to prevent the cathode nanoparticles from being dissolved and thus improve the cyclic performance.[7] Several groups deposited yttria-stabilized zirconia through the ALD cycles of Y_2O_3 and ZrO_2 to develop thin electrolyte films with better conduction of oxygen ions in solid oxide fuel cells.[6] All these examples highlight how the ALD technique can be commonly applied to a broad array of applications. These studies also emphasize that understanding the fundamental chemistry of the ALD processes would be needed to optimize the performance of the ALD-prepared thin films.

As the most well-known ALD chemistry, the ALD process for Al_2O_3 thin films is often performed using trimethylaluminum (TMA) and water (H_2O) as precursors of aluminum and oxygen, respectively, via the following two half-cycles.[8]

TMA-dosed half-cycle (n = 1 or 2):

$$n\mathrm{s-OH} + \mathrm{Al}(CH_3)_3 \rightarrow \mathrm{s-O}_n Al(CH_3)_{3-n} + nCH_4(\mathrm{g}) \quad (1)$$

H_2O-dosed half-cycle:

$$\mathrm{s-O}_n Al(CH_3)_{3-n} + (3-n)\mathrm{H_2O(g)} \rightarrow \mathrm{s-O}_n Al(\mathrm{OH})_{3-n} + (3-n)CH_4\ (\mathrm{g}) \quad (2)$$

where "s" depicts the alumina surface. As described in the reaction schemes, each precursor is dosed onto the substrate in which the precursor molecules can react with the active adsorption sites (e.g., hydroxyls or methylaluminum species) on the surface. These ligand-exchange reactions are summarized by the alternating condensation (TMA-dosed half-cycle) and hydrolysis (H_2O-dosed half-cycle) via the proton transfer between the active adsorption sites and precursor molecules. Various studies on the ALD mechanism of Al_2O_3 have been conducted to understand the ALD chemistry.[6,9−12] Utke and

Received: May 11, 2020
Revised: June 17, 2020
Accepted: June 19, 2020
Published: June 19, 2020

https://dx.doi.org/10.1021/acs.iecr.0c02382
Ind. Eng. Chem. Res. 2020, 59, 13325−13332

co-workers explored the ALD mechanisms in a variety of scenarios associated with the TMA- and H_2O-dosed half-cycles.[13] They highlighted that the unreacted hydroxyl groups generated during the ALD process would be due to the steric hindrance by neighboring TMA adsorbates in monodentate configurations. Gakis *et al.*[14] investigated the growth per cycle (GPC) of ALD by changing process temperatures. They reported that the decrease in the GPC at higher temperatures would be due to the decrease in the hydroxyl groups on the surfaces.[14] Sandupatla *et al.* investigated the growth inhibition behaviors observed during the alumina ALD on silica substrates.[15] Despite all these significant efforts, the fundamental understanding on the mechanistic pathway of the ALD process is still lacking because most previous studies did not consider the possibility of the presence of dimeric TMA adsorbates, even though TMA has the thermodynamic balance between its monomeric and dimeric formations both in vapor and liquid phases.[16] Indeed, Hackler *et al.* recently identified dimeric methylalumina species on silver surfaces using *operando* surface-enhanced Raman spectroscopy.[17] Potts *et al.* also discussed the dimeric nature of $[Al(CH_3)_2(l\text{-}O^iPr)]_2$ (DMAI, ^{i}Pr = isopropyl), an alternative Al precursor to TMA for remote plasma-enhanced and thermal ALD of Al_2O_3 thin films.[18]

Recently, the first-principles density functional theory (DFT) calculations have emerged to be a promising technique that can be employed to understand the ALD processes of metal oxides. Chen *et al.* employed the DFT modeling approach to understand the decomposition behaviors of TMA molecules during the Al_2O_3 ALD on $LiMn_2O_4$ cathodes for lithium-ion batteries.[19] Elliott and co-workers used the DFT modeling approach to study the reaction mechanisms and resultant intermediates/byproducts on the TMA-chemisorbed alumina under the O_2 plasma during the alumina ALD process.[23] They found that formaldehyde (CH_2O) was the most frequently observed gaseous byproduct when the oxygen atom reached on the methyl surface. Seo *et al.* also employed the DFT calculations to study the time-evolved movements of TMA species absorbed on the surface of Al_2O_3 at different process conditions, such as TMA-dosed pressure, process temperature, and exposure time.[20] They demonstrated that the TMA-dosed pressure would be the critical factor in determining the density of TMA molecules chemisorbed on the surface. All these elucidate the potential of the DFT modeling approach as an efficient way to understand the chemistry and mechanistic flow of the ALD-assisted process for the generation of Al_2O_3 thin films.

In this work, we employ the DFT modeling approach to explore the chemisorption behaviors of TMA molecules on the active adsorption sites of the Al_2O_3 surfaces and to investigate the possibility of the dimeric adsorption of TMA during the TMA-dosed half-cycle. The thermodynamic characteristics associated with the subsequent H_2O-dosed half-cycle are further investigated to understand the ALD chemistry. Through this study, we highlight that TMA molecules would prefer to be chemisorbed on the surfaces in a monomeric form rather than in a dimeric form. It is further verified that the thermodynamic profile during the H_2O-dosed half-cycle would strongly rely on the structural geometry (e.g., monodentate vs bidentate) of the TMA species chemisorbed during the previous TMA-dosed half-cycle.

COMPUTATIONAL METHODS

All the DFT calculations were performed using the Quantum Espresso package with Perdew–Burke–Ernzerhof (PBE) generalized gradient approximation functional.[21] The core electrons of each atom were described by ultrasoft pseudopotential. Energy cutoffs for wave function (680 eV) and charge density (6530 eV) were confirmed to be large enough to reliably predict the electronic structures. The bulk structure of the Al_2O_3 structure was geometrically optimized, allowing supercell and all atoms in the cell to fully relax until the forces on all atoms were less than 0.01 eV/Å. The $Al_2O_3(0001)$ surface model was further developed through the cleavage of the optimized bulk structure followed by the hydroxylation of the surface dangling bonds. Note that the $Al_2O_3(0001)$ surface was selected because the surface was the most stable in the thermodynamic point of view, exhibiting the lowest surface energy among possible low Miller index surfaces. The surface optimization was performed via the same procedure as the bulk optimization, except fixing the supercell. The resultant surface model contains six Al–O layers with a vacuum thickness of 30 Å. Such a large vacuum thickness would prevent the interaction between neighboring slab images, leading to the negligible effect of the dipole moment in the surface model.

Relative Thermodynamic Stability of TMA Adsorbates. Five monomeric species (MS) and two dimeric species (DS) models depict the TMA species chemisorbed on the developed $Al_2O_3(0001)$ surface in monomeric and dimeric forms, respectively. The mechanisms for the MS and DS formation are described by

$$\text{MS: } (m+n)\text{s} - \text{OH} + 2\text{Al}(CH_3)_3 \rightarrow \text{s} - \text{O}_m Al(CH_3)_{3-m} + \text{s} - \text{O}_n Al(CH_3)_{3-n} + (m+n)CH_4(\text{g}) \quad (3)$$

$$\text{DS: } (m+n)\text{s} - \text{OH} + 2\text{Al}(CH_3)_3 \rightarrow m\text{s} - \text{OH} + \text{s} - \text{O}_n\text{Al}_2(CH_3)_{6-n} + nCH_4(\text{g}) \quad (4)$$

where m and n are either 1 or 2. In the following, the methyl-terminated surfaces, produced by the reactions of eq 3 and/or eq 4, are expressed as "TMA-chemisorbed surface". The formation energy (E_f) per two TMA monomers for each of the seven species models was calculated by

$$\text{MS: } E_f = E(\text{s} - \text{O}_m Al(CH_3)_{3-m}) + E(\text{s} - \text{O}_n Al(CH_3)_{3-n}) + (m+n)E(CH_4) - (m+n)E(\text{s} - \text{OH}) - 2E(Al(CH_3)_3) \quad (5)$$

$$\text{DS: } E_f = mE(\text{s} - \text{OH}) + E(\text{s} - \text{O}_n Al_2(CH_3)_{6-n}) + nE(CH_4) - (m+n)E(\text{s} - \text{OH}) - 2E(\text{Al}(CH_3)_3) \quad (6)$$

Thermodynamic Profile during H_2O-Dosed Half-Cycle. Surface models, which were fully covered by the chemisorbed TMA species, were developed following a set of conditions imposed by the nature of the ALD process: (i) Each TMA adsorbate has to occupy its own space without any steric hindrance by neighboring TMA adsorbates. (ii) The aforementioned condition has to be satisfied throughout the

https://dx.doi.org/10.1021/acs.iecr.0c02382
Ind. Eng. Chem. Res. 2020, 59, 13325–13332

entire space extended by neighboring images of the supercell (periodicity). Water molecules were subsequently added on the developed surfaces one by one, exploring the thermodynamically stable configurations, to study the change in the thermodynamic quantity (i.e., formation energy) during the half-cycle. The sequential chemisorption energy (E_b) of H_2O to the TMA-chemisorbed $Al_2O_3(0001)$ surface is computed by

$$E_b = E(\text{Al}_2\text{O}_3 \text{ surface with } (m-1) \text{ methyl groups and } (n+1) \text{ hydroxyls}) + E(CH_4) - E(\text{Al}_2\text{O}_3 \text{ surface with } m \text{ methyl groups and } n \text{ hydroxyls}) - E(\text{H}_2\text{O}) \quad (7)$$

where m is the number of the methyl groups on the TMA-chemisorbed surface after the nth hydroxylation event ($m = 4$ for the MS2 model and $m = 9$ for the MS3 model before the H_2O-dosed half-cycle) and n is the number of the hydroxylation events in the sequential adsorption of water (see the following section for the description of MS2 and MS3 models).

RESULTS AND DISCUSSION

Table S1 in the Supporting Information provides the structural information on the bulk and slab surface models developed in this study. As listed in the table, the structural information (e.g., lattice parameters in the bulk Al_2O_3 model and bond length and angle in the hydroxylated Al_2O_3 surface model) agrees well with their theoretical/experimental values reported in previous studies.[22−25] The computational protocol employed in this study to describe the binding properties of precursors (i.e., TMA and H_2O) is further validated by a preliminary calculation. Nguyen recently studied the adsorption energy of H_2O on the $Al_2O_3(0001)$ surface using the same protocol as ours (Quantum Espresso package with PBE functional and ultrasoft pseudopotential).[26] Our preliminary calculation on the H_2O adsorption thermodynamics on the same surface site predicts the adsorption energy of −1.12 eV, which agrees well with the reported value (−1.13 eV).[26] This enables us to draw concrete conclusions from the ALD mechanisms based on our computational protocol.

MS versus DS for TMA Adsorbates on the $Al_2O_3(0001)$ Surface. In general, it is believed that TMA molecules are chemisorbed in a monomeric form during the TMA-dosed half-cycles. However, a couple of studies have reported the possible formation of dimeric TMA adsorbates during the TMA-dosed half-cycle. For instance, Van Duyne and co-workers recently employed a technique of *operando* surface-enhanced Raman spectroscopy (SERS) combined with DFT to explore the ALD-based growth behaviors of alumina on bare silver film over nanosphere substrates.[27] They highlighted that TMA dimeric adsorbates would be possibly formed on the surface during the alumina ALD process. The same research group employed SERS to understand the structural formation of methylalumina species observed on a SERS-active silver surface during dosing TMA and dimethylaluminum chloride precursors on the surface.[17] They highlighted a possible formation of dimeric structures on the surface based on the vibrational modes describing bridging moieties. According to our DFT-based calculations, the dimeric TMA species has the formation energy lower by 73.7 kJ/mol than the monomeric TMA species and this somewhat support their claims (see Figure 1a). All these finally raise a fundamental question on

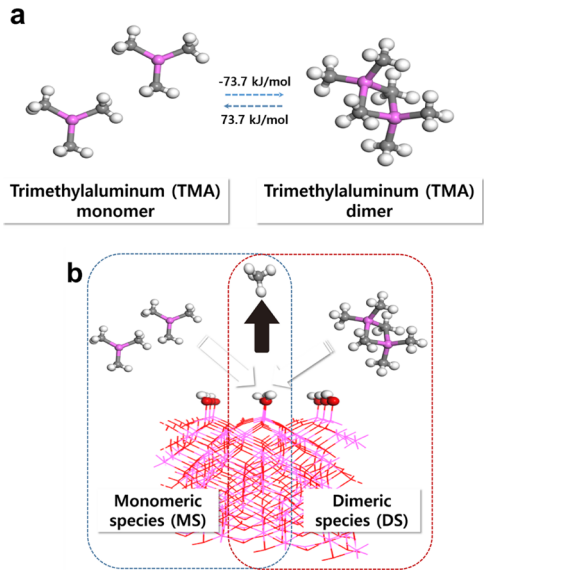

Figure 1. Comparison of monomeric (MS) and dimeric (DS) species. (a) Thermodynamic energy difference between two trimethylaluminum (TMA) monomers and a TMA dimer in the gaseous phase. (b) Illustrated formation of MS and DS for TMA-based atomic layer deposition. Atoms with gray, white, red, and purple in color depict carbon, hydrogen, oxygen, and silicon, respectively.

"MS versus DS for TMA species chemisorbed on $Al_2O_3(0001)$ surfaces" (see Figure 1b). Note that the mechanism of the TMA-dosed half-cycle would strongly rely on whether the chemisorbed TMA species are either monomeric or dimeric species on the surfaces. This question has to be therefore answered to comprehensively understand the mechanistic behaviors of the TMA/H_2O-dosed ALD process.

A total of seven TMA surface species can be designed to systematically study the thermodynamic preference associated with the formation type of the chemisorbed TMA species. Figure 2 shows structural models of all these feasible TMA surface species (i.e., five MS and two DS models). The models have a surface coverage of 1.13−1.15 TMA/nm^2, indicating

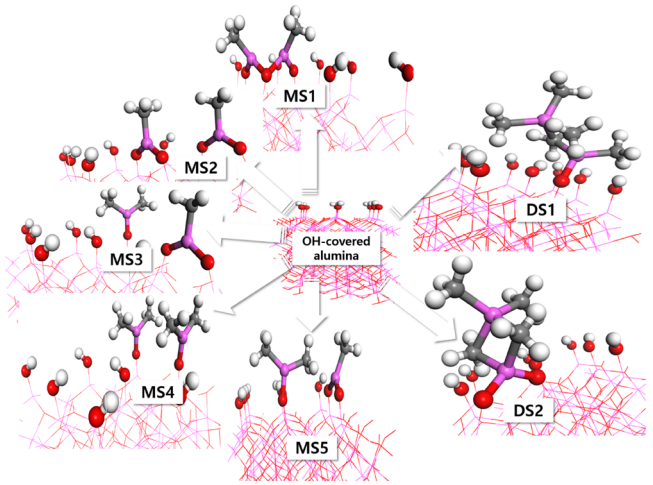

Figure 2. Type of feasible MS and DS structures. Chemical structures of five MS and two DS possibly formed after the TMA-incorporated cycle in the atomic layer deposition process. Atoms with gray, white, red, and purple in color depict carbon, hydrogen, oxygen, and silicon, respectively.

https://dx.doi.org/10.1021/acs.iecr.0c02382
Ind. Eng. Chem. Res. 2020, 59, 13325−13332

that the surface models are large enough to prevent the interaction of TMA adsorbates on neighboring slab surfaces. Two primary factors, namely, (i) monomeric/dimeric formations and (ii) monodentate/bidentate configurations, are considered for the design of the TMA-chemisorbed surfaces. The chemical structures for the five different models having monomeric TMA formations are illustrated on the left side of Figure 2. First of all, MS1 and MS2 models allow two neighboring TMA adsorbates to be chemically bonded to three and four oxygen atoms of the $Al_2O_3(0001)$ surface in bidentate configurations, respectively. Note that the two monomeric TMA adsorbates in the MS1 model would share an oxygen atom during the chemisorption. In contrast, each MS3 and MS5 model has two neighboring TMA adsorbates chemisorbed on the surface: one in the monodentate configuration and the other in the bidentate configuration. It is worth noting that the MS3 model has no interaction between the two monomeric TMA adsorbates, while a methyl group of the monodentate configuration in the MS5 model weakly interacts with the Al atom of the bidentate configuration. The MS4 model shows two neighboring TMA species chemisorbed on the surface in a monodentate configuration. Two surface species in dimeric TMA formations (DS1 and DS2 models) are chemisorbed on the surface in a monodentate or bidentate manner as shown on the right side of Figure 2.

As described in the reaction schemes (eqs 3 and 4), the aforementioned models are developed using the ALD-mimicked process in which two TMA fragments are dosed on the hydroxylated $Al_2O_3(0001)$ surface. The formation energies of the seven models are therefore computed using eqs 5 and 6 (see Figure 3 and Table S2 in the Supporting Information). The detailed reaction schemes for MS and DS models are also visually illustrated in Figures S1 and S2 in the Supporting Information, respectively. In general, bidentate configurations are predicted to be more stable than monodentate configurations owing to the higher connectivity between Al and surface O atoms for the former. It is also unambiguous to see that the TMA species on the surface would thermodynamically prefer to be chemisorbed in a monomeric form rather than in a dimeric form. The formation energies for four MS-based models (MS2−MS5) are predicted to be ranged within −3.39 to −4.81 eV/2 TMA, which would be more negative than the values (−2.41 and − 2.89 eV/2 TMA) for DS-based models. It is further noted that the bond lengths (2.1 Å) of Al and C binding two monomeric species in the DS models are greater by 0.2 Å than the other Al−C bond lengths in the MS and DS models (see Tables 1 and 2).

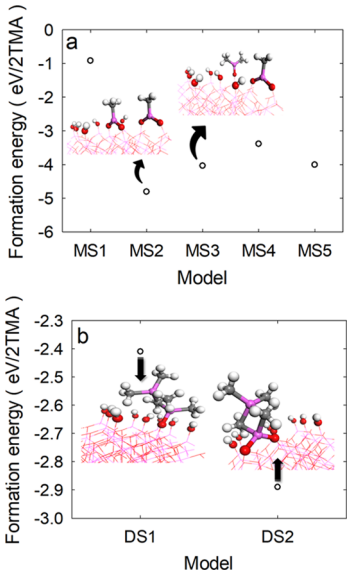

Figure 3. Thermodynamics of MS and DS. The DFT-calculated total energies of (a) five MS and (b) two DS models.

Table 1. Structural Characteristics for Five MS Models Feasible from the TMA-Based Atomic Layer Deposition Cycle[a]

model		MS1	MS2	MS3	MS4	MS5
angle (°)	$C_1-Al_1-O_1$	116.6	116.7	116.7	118.1	117.1
	$C_1-Al_1-O_2$	110.7	117.0	117.0		117.7
	$C_2-Al_1-O_1$				118.1	
	$C_2-Al_2-O_2$	117.0				
	$C_2-Al_2-O_3$	121.0	115.8	117.6		112.4
	$C_2-Al_2-O_4$		117.2			
	$C_3-Al_2-O_2$				117.6	
	$C_3-Al_2-O_3$			118.9		121.2
	$C_4-Al_2-O_2$				118.3	
	$C_1-Al_1-C_2$				123.7	
	$C_2-Al_2-C_3$			123.5		126.3
	$C_3-Al_2-C_4$				124.1	
	$O_1-Al_1-O_2$	121.3	126.3	126.3		123.4
	$O_2-Al_2-O_3$	111.2				
	$O_3-Al_2-O_4$		126.9			
	$Al_1-O_2-Al_2$	85.1				
distance (Å)	C_1-Al_1	1.97	1.95	1.95	1.96	1.96
	C_2-Al_1				1.96	
	C_2-Al_2	1.96	1.95	1.96		1.96
	C_3-Al_2			1.96	1.96	1.96
	C_4-Al_2				1.96	
	Al_1-O_1	1.73	1.73	1.73	1.71	1.75
	Al_1-O_2	1.97	1.74	1.74		1.76
	Al_2-O_2	1.94			1.70	
	Al_2-O_3	1.73	1.74	1.71		1.70
	Al_2-O_4		1.74			

[a]The identity of each atomic label is shown in Figure S3 in the Supporting Information.

Considering the relative thermodynamic stability of the models in terms of the bond geometry, the presence of a TMA molecule weakly maintained by these loose bonds for each DS model would be a critical indicator to describe the characteristics of the DS models less stable than the MS models. Interestingly, the MS1 model, in which a surface oxygen atom is shared for the chemisorption of the two monomeric TMA species, is thermodynamically less stable than any other models introduced in this work. Although such an MS1 model was adopted to propose a mechanism for the chemisorption of a TMA species in a previous study,[28] this work reveals that each surface oxygen atom is ideally capable of fully interacting with only one Al atom to release one methane molecule. It is further reported from the previous study that the MS1 model would follow the reaction scheme of eq 8 and the formation energy of eq 9 instead of eqs 3 and 5:

https://dx.doi.org/10.1021/acs.iecr.0c02382
Ind. Eng. Chem. Res. 2020, 59, 13325−13332

Table 2. Structural Characteristics for Two DS Models Feasible from the TMA-Based Atomic Layer Deposition Cycle[a]

model		DS1	DS2
angle (°)	$O_1-Al_2-C_3$	109.6	103.2
	$O_1-Al_2-C_4$	109.3	107.6
	$O_1-Al_2-C_5$	122.0	
	$O_2-Al_2-C_3$		106.0
	$O_2-Al_2-C_4$		107.8
	$O_1-Al_2-O_2$		126.1
	$C_1-Al_1-C_2$	121.5	120.7
	$C_1-Al_1-C_3$	107.8	105.0
	$C_1-Al_1-C_4$	110.4	107.6
	$C_2-Al_1-C_3$	106.4	109.6
	$C_2-Al_1-C_4$	105.0	110.3
	$C_3-Al_1-C_4$	104.5	101.9
	$C_3-Al_2-C_4$	105.0	104.1
	$C_3-Al_2-C_5$	102.2	
	$C_4-Al_2-C_5$	107.5	
	$Al_1-C_3-Al_2$	75.0	75.0
	$Al_1-C_4-Al_2$	75.2	75.3
distance (Å)	C_1-Al_1	1.97	1.97
	C_2-Al_1	1.97	1.97
	C_3-Al_1	2.14	2.14
	C_4-Al_1	2.15	2.16
	C_3-Al_2	2.14	2.14
	C_4-Al_2	2.13	2.10
	C_5-Al_2	1.97	
	O_1-Al_2	1.72	1.74
	O_2-Al_2		1.75

[a]The identity of each atomic label is shown in Figure S3 in the Supporting Information.

$$3s - \mathrm{OH} + 2\mathrm{Al}(CH_3)_3 \rightarrow \mathrm{s} - \mathrm{O_3(Al}(CH_3))_2 + 2CH_4(\mathrm{g}) + \mathrm{C_2H_4(g)} + 3/2H_2(\mathrm{g}) \quad (8)$$

$$E_f = E(\mathrm{s} - \mathrm{O_3(Al}(CH_3))_2) + 2E(CH_4) + E(\mathrm{C_2H_4}) + 3/2E(\mathrm{H_2}) - 3E(\mathrm{s} - \mathrm{OH}) - 2E(Al(CH_3)_3) \quad (9)$$

The detailed reaction scheme is visualized in Figure S1a in the Supporting Information. It is also verified that the release of ethylene and hydrogen molecules in addition to methane molecules in the reaction scheme of eq 8 would be thermodynamically less favored as compared with the release of only methane molecules in the other models. The characteristics of the MS1 model less stable than the other MS and DS models can be also rationalized by its unique structural characteristics. The bond lengths (1.9−2.0 Å) between Al and the sharing O in the MS1 model are relatively longer than the other Al−O bond lengths (1.7−1.8 Å), indicating the weakened structural stability (see Tables 1 and 2).

Another highlighted feature from Figure 3 and Table S2 in the Supporting Information is that the MS2 model would be the most stable configuration, exhibiting a formation energy of −4.81 eV/2 TMA. This value is more negative by ∼0.8 eV/2 TMA than MS3 and MS5 models having the second-lowest formation energies. Such high stability is primarily due to the geometrically balanced characteristics of the MS2 model as compared with the other models. In contrast, the MS3 and MS5 models have similar stability, indicating that the energy reward arising from the weak interaction between the two neighboring TMA adsorbates would be canceled off by the energy loss due to the structural elongation for the interaction. It is concluded from all these that the TMA-dosed ALD half-cycle will be dominated by the MS2-type chemisorption of monomeric TMA species in the thermodynamic point of view. However, either MS3- or MS5-type chemisorption is also predicted to be observed with a portion depending on the ALD temperature during the TMA-dosed half-cycle. According to the temperature-induced kinetic effects, the dehydroxylation of surface hydroxyl groups with high vibrational energies at an increased temperature would cause a decrease in the number of the hydroxyl adsorption sites and might geometrically suppress the bidentate configuration of TMA species. This leads to an increase in the ratio of the MS3- or MS5-type chemisorption relative to the MS2-type chemisorption. Ritala *et al.* used an approach of *in situ* characterization combined with a mass spectrometer to investigate the temperature-dependent ALD processes for the generation of Al_2O_3 thin films.[29] They highlighted that the bidentate-type TMA configuration (i.e., MS2 model) would be more dominant at a lower deposition temperature, exhibiting the chemisorption of almost all the TMA species in the bidentate configuration even at 150 °C. Considering the intrinsic property of the DFT method, this experiment confirms the reliability of our computational results.

H_2O-Dosed Half-Cycle on the TMA-Chemisorbed Al_2O_3(0001) Surface. In the previous section, it is unveiled that the MS2-type chemisorption would be dominantly occupied with a small percentage of MS3- and MS5-type deposition during the TMA-dosed half-cycle in the thermodynamic point of view. Based on this information, we now turn to the next half-cycle, namely, the H_2O-dosed half-cycle. We specifically designed two types of TMA-chemisorbed Al_2O_3(0001) surface models, assuming that TMA species would be chemisorbed in the form of either MS2 or MS3 model during the TMA-dosed half-cycle. Figure 4 illustrates the ALD processes following the MS2- or MS3-type formation of TMA adsorbates in the TMA-dosed half-cycle and the subsequent hydroxylation of the TMA adsorbates in the H_2O-dosed half-cycle.

The hydroxylation in the H_2O-dosed half-cycle is relatively a simple process as compared with the TMA chemisorption process in the TMA-dosed half-cycle. During the process, each water molecule would interact with a methyl group of a chemisorbed TMA species to replace the methyl group into a hydroxyl group through the ligand exchange and release a methane molecule. A critical question on the H_2O-dosed half-

https://dx.doi.org/10.1021/acs.iecr.0c02382
Ind. Eng. Chem. Res. 2020, 59, 13325−13332

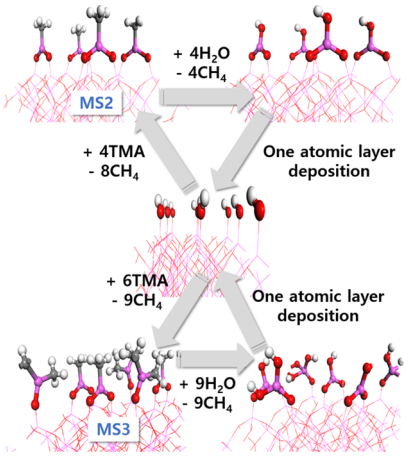

Figure 4. Atomic layer deposition. The TMA/H_2O-based atomic layer deposition processes for MS2 and MS4 cases.

cycle would be therefore related to how the water molecules would be chemically adsorbed on the TMA-chemisorbed surface in the thermodynamic point of view. The profiles for the sequential chemisorption energy of H_2O on the TMA-chemisorbed surface are shown in Figure 5a (MS2) and Figure

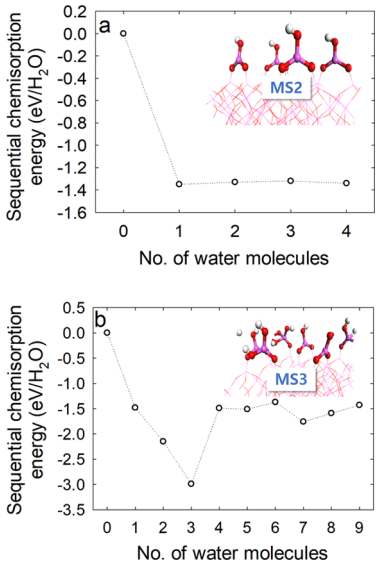

Figure 5. Thermodynamic energy profiles for atomic layer deposition processes. The change in the DFT-calculated sequential chemisorption energy during the water-based atomic layer deposition cycle for (a) MS2 and (b) MS3 models.

5b (MS3) with the specific values in Table S3 (MS2) and Table S4 (MS3) in the Supporting Information. The sequential chemisorption processes are visualized in Figures S4 and S5 in the Supporting Information in detail. Note that water molecules would be sequentially chemisorbed on the most favorable active adsorption sites through the reaction with methyl groups of the TMA adsorbates under the condition of excluding the kinetic effect. It should be also noted that the MS2 and MS3 models have surface coverages of 2.3 and 5.1 OH/nm^2 after the full chemisorption, respectively. It is clear to see from the profiles of formation energy in Figure 5 that water molecules are exothermically chemisorbed on the surfaces during the H_2O-dosed half-cycle.

The most striking observation from Figure 5 and Tables S3 and S4 in the Supporting Information is that the energy profile for the sequential chemisorption of water molecules strongly relies on the configuration of TMA adsorbates on the surface at the early stage of the H_2O-dosed half-cycle. The chemisorption of water molecules on the TMA (MS2)-chemisorbed surface exhibits a constant energy profile within the range of −1.32 to −1.35 eV/H_2O, regardless of the number of chemisorbed water molecules (i.e., the number of the hydroxylation events in the sequential chemisorption of water). Considering that all the TMA species are uniformly chemisorbed on the bare surface in a bidentate configuration, all the active adsorption sites (monomethylaluminum groups) for the subsequent chemisorption of water molecules would be identical in the thermodynamic point of view (see Figure 4 and Figures S4 and S5). In addition, the space between neighboring TMA adsorbates is large enough to neglect the self-interaction between the water molecules chemisorbed on the neighboring TMA adsorbates (see Figure S5). The constant energy profile for the TMA (MS2)-chemisorbed surface can be reasonably explained from all this evidence. In contrast to the MS2 configuration, the active adsorption sites for the chemisorption of water molecules on the TMA (MS3)-chemisorbed surface are not identical due to the co-existence of monodentate and bidentate configurations. For the MS3 configuration, the sequential chemisorption energy of water changes from −1.48 to −2.99 eV/H_2O with the number of hydroxyls chemisorbed on the surface until the first three water molecules are hydroxylated on the surface. This implies that the chemisorption of a water molecule would be thermodynamically assisted by the previously chemisorbed water molecule(s). The chemisorption of the fourth water molecule leads to a sudden change in the chemisorption energy toward −1.49 eV/H_2O. Further chemisorption of water molecules on the surface does not significantly affect the chemisorption energy.

The distinctive H_2O chemisorption behavior on the TMA (MS3)-chemisorbed Al_2O_3(0001) surface is related to the distribution of the TMA adsorbates. Note that the surface contains three pairs of the monodentate dimethylaluminum and the bidentate monomethylaluminum adsorbates (see Figure S5b in the Supporting Information). Each of the first three water molecules independently interacts with a methyl group in each of the three monodentate dimethylaluminum adsorbates to form a hydroxyl group with the release of methane gas. The resultant accumulation of hydroxyl groups on the surface would lead to the enhancement of the sequential chemisorption energy. Interestingly, the first three hydroxyl groups prefer to be placed on monodentate-type TMA configurations, leading to all the three monodentate-type TMA species coordinating with a hydroxyl group. The fourth water molecule is predicted to interact with a methyl group in a monodentate-type TMA configuration (i.e., methylhydroxylaluminum group), although the configuration already has a hydroxyl group chemically bound in its space. This implies its preference for the monodentate configuration. The resultant co-existence of two hydroxyl groups chemically bound in an identical monodentate-type configuration leads to a sudden increase in the sequential chemisorption energy. The fifth hydroxyl group is placed in a bidentate-type configuration, forming a hydrogen bond with a hydroxyl group in its neighboring monodentate-type configuration. The surface model is stabilized by the hydrogen bond, exhibiting the slight

https://dx.doi.org/10.1021/acs.iecr.0c02382
Ind. Eng. Chem. Res. 2020, 59, 13325−13332

decrease in the sequential chemisorption energy from −1.49 to −1.51 eV/H_2O. Further chemisorption of water molecules on the surface would eventually converge the sequential chemisorption energy to ∼1.5 eV/H_2O. Therefore, the thermodynamic feasibility of the water molecules would not be significantly varied after the early stage of the sequential hydroxylation because an excessive amount of water vapor would be dosed in the H_2O-dosed half-cycle of a real ALD process.

CONCLUSIONS

In this study, we employed the first-principles DFT calculations to understand the reaction schemes of the TMA/H_2O-dosed ALD process and their thermodynamics. First of all, seven different models, namely, five MS and two DS models, were systematically designed to unveil the configurations of the TMA species chemisorbed on the hydroxylated Al_2O_3(0001) surfaces during the TMA-dosed half-cycle of the ALD process. It was highlighted from the investigation that the MS models would be generally more stable than the DS models. Among the five MS models, a model containing two monomeric TMA adsorbates with structurally balanced bidentate configurations was predicted to have the lowest formation energy, indicating its exceptionally stable characteristics in the thermodynamic point of view. The subsequent chemisorption behaviors of water molecules on the TMA-chemisorbed Al_2O_3(0001) surfaces were mimicked to further explore the reaction mechanism of the H_2O-dosed half-cycle and its thermodynamics. The primary conclusions drawn from this study are summarized below. (1) The energy profile for the sequential chemisorption of water molecules in the H_2O-dosed half-cycle would strongly rely on the configurations of TMA species chemisorbed during the previous TMA-dosed half-cycle. The chemisorption of water molecules on the TMA (MS2)-chemisorbed surface exhibits a constant energy profile for the sequential chemisorption. On the other hand, for the TMA (MS3)-chemisorbed surface model, the sequential chemisorption energy is predicted to experience an initial decrease (i.e., higher chemisorption ability) followed by a sudden increase (i.e., lower chemisorption ability) and then a negligible variation as the number of the chemisorbed hydroxyl groups increases. (2) Despite the TMA adsorbate configuration-dependent variation in the sequential chemisorption energy at the early stage of the H_2O-dosed half-cycle, the energy profile would eventually become independent on the density of the surface hydroxyl groups. This suggests that the thermodynamic feasibility of the water molecules chemisorbed after the early stage of the H_2O-dosed half-cycle would not be significantly varied in real ALD processes. (3) In each half-cycle, precursor molecules are assumed to be independently chemisorbed on the surfaces without being disturbed by neighboring precursor molecules and/or chemisorbed species. Thus, this study provides an insight on the ALD mechanism in the thermodynamic point of view.

All these conclusions drawn in this study are based on the DFT calculations at 0 K with no consideration of temperature-dependent vibrational and entropic effects on the free energy. However, it is worth noting that the temperature-dependence of the free energy will be significant only if the difference in the thermodynamic stability between models is small. The free energy difference between MS models and DS models is large enough to ignore the temperature dependence. In addition, the MS2 model with the highest thermodynamic stability has the DFT-calculated formation energy (−464 kJ/mol of 2TMA), which is at least 74 kJ/mol of 2TMA lower than the other models. Likewise, the studies on the sequential chemisorption of H_2O during the H_2O-dosed half-cycle for MS2 and MS3 models mainly focus on the trend in the chemisorption energy with the increase in the number of the chemisorbed adsorbates rather than the chemisorption energies themselves. Therefore, the conclusions would not be significantly changed even though the temperature-dependent vibrational and entropic effects are considered.

ASSOCIATED CONTENT

Supporting Information

The Supporting Information is available free of charge at https://pubs.acs.org/doi/10.1021/acs.iecr.0c02382.

TMA/H_2O-dosed ALD mechanisms and relevant structural information for MS and DS models and thermodynamic information on the TMA and H_2O chemisorption (PDF)

AUTHOR INFORMATION

Corresponding Authors

Yo-Sep Min − *Division of Chemical Engineering, Konkuk University, Seoul 05029, The Republic of Korea;* orcid.org/0000-0002-2340-3633; Email: ysmin@konkuk.ac.kr

Ki Chul Kim − *Division of Chemical Engineering, Konkuk University, Seoul 05029, The Republic of Korea;* Email: kich2018@konkuk.ac.kr

Authors

Jae Won Choi − *Division of Chemical Engineering, Konkuk University, Seoul 05029, The Republic of Korea*

So-Yeon Ham − *Division of Chemical Engineering, Konkuk University, Seoul 05029, The Republic of Korea*

Suhyun Lee − *Division of Chemical Engineering, Konkuk University, Seoul 05029, The Republic of Korea*

Da-Som Shin − *Division of Chemical Engineering, Konkuk University, Seoul 05029, The Republic of Korea*

Complete contact information is available at: https://pubs.acs.org/10.1021/acs.iecr.0c02382

Notes

The authors declare no competing financial interest.

ACKNOWLEDGMENTS

This work was supported by the Samsung Research Funding & Incubation Center of Samsung Electronics (SFRC-MA1801-01). This paper was supported by the Konkuk University Researcher Fund in 2018.

REFERENCES

(1) George, S. M. Atomic layer deposition: an overview. *Chem. Rev.* **2010**, *110*, 111−131.

(2) S. I. Association, *International technology roadmap for semiconductors* (2007 Edition), http://www.itrs.net/ ed. 2007 ed.

(3) Parsons, G. N.; Elam, J. W.; George, S. M.; Haukka, S.; Jeon, H.; Kessels, W. M. M. (. E.).; Leskelä, M.; Poodt, P.; Ritala, M.; Rossnagel, S. M. History of atomic layer deposition and its relationship with the American Vacuum Society. *J. Vac. Sci. Technol., A* **2013**, *31*, No. 050818.

(4) Ott, A. W.; Klaus, J. W.; Johnson, J. M.; George, S. M. Al3O3 thin film growth on Si (100) using binary reaction sequence chemistry. *Thin Solid Films* **1997**, *292*, 135−144.
(5) Ott, A. W.; McCarley, K. C.; Klaus, J. W.; Way, J. D.; George, S. M. Atomic layer controlled deposition of Al2O3 films using binary reaction sequence chemistry. *Appl. Surf. Sci.* **1996**, *107*, 128−136.
(6) Kessels, W. M. M.; Knoops, H. C. M.; Weber, M. J.; Mackus, A. J. M.; Creatore, M. Atomic layer deposition of nanomaterials for Li-ion batteries, fuel cells, and solar cells. *Mater. Matters* **2013**, *8*, 117−117.
(7) Scott, I. D.; Jung, Y. S.; Cavanagh, A. S.; Yan, Y.; Dillon, A. C.; George, S. M.; Lee, S.-H. Ultrathin coatings on nano-LiCoO2 for Li-Ion vehicular applications. *Nano Lett.* **2011**, *11*, 414−418.
(8) Xu, Y.; Musgrave, C. B. A DFT study of the Al2O3 atomic layer deposition on SAMs: effect of SAM termination. *Chem. Mater.* **2004**, *16*, 646−653.
(9) Dillon, A. C.; Ott, A. W.; Way, J. D.; George, S. M. Surface chemistry of Al_2O_3 deposition using $Al(CH_3)_3$ and H_2O in a binary reaction sequence. *Surf. Sci.* **1995**, *322*, 230−242.
(10) Yun, S. J.; Lee, K.-H.; Skarp, J.; Kim, H.-R.; Nam, K.-S. Dependence of atomic layer-deposited Al2O3 films characteristics on growth temperature and Al precursors of Al(CH3)3 and AlCl3. *J. Vac. Sci. Technol., A* **1997**, *15*, 2993−2997.
(11) Kukli, K.; Ritala, M.; Leskelä, M.; Jokinen, J. Atomic layer epitaxy growth of aluminum oxide thin films from a novel Al(CH3)2Cl precursor and H2O. *J. Vac. Sci. Technol., A* **1997**, *15*, 2214−2218.
(12) FAN, J.-F.; SUGIOKA, K.; TOYODA, K. Low-temperature growth of thin films of Al2O3 by sequential surface chemical reaction of trimethylaluminum and H2O2. *Jpn. J. Appl. Phys.* **1991**, *30*, L1139−L1141.
(13) Guerra-Nuñez, C.; Döbeli, M.; Michler, J.; Utke, I. Reaction and growth mechanisms in Al2O3deposited via atomic layer deposition: elucidating the hydrogen source. *Chem. Mater.* **2017**, *29*, 8690−8703.
(14) Gakis, G. P.; Vergnes, H.; Scheid, E.; Vahlas, C.; Boudouvis, A. G.; Caussat, B. Detailed investigation of the surface mechanisms and their interplay with transport phenomena in alumina atomic layer deposition from TMA and water. *Chem. Eng. Sci.* **2019**, *195*, 399−412.
(15) Sandupatla, A. S.; Alexopoulos, K.; Reyniers, M.-F.; Marin, G. B. DFT investigation into alumina ALD growth inhibition on hydroxylated amorphous silica surface. *J. Phys. Chem. C* **2015**, *119*, 18380−18388.
(16) Laubengayer, A. W.; Gilliam, W. F. The alkyls of the third group elements. I. vapor phase studies of the alkyls of aluminum, gallium and indium[1]. *J. Am. Chem. Soc.* **1941**, *63*, 477−479.
(17) Hackler, R. A.; McAnally, M. O.; Schatz, G. C.; Stair, P. C.; Van Duyne, R. P. Identification of dimeric methylalumina surface Species during atomic layer deposition using operando surface-enhanced Raman spectroscopy. *J. Am. Chem. Soc.* **2017**, *139*, 2456−2463.
(18) Potts, S. E.; Dingemans, G.; Lachaud, C.; Kessels, W. M. M. Plasma-enhanced and thermal atomic layer deposition of Al2O3 using dimethylaluminum isopropoxide, [Al(CH3)2(μ-OiPr)]2, as an alternative aluminum precursor. *J. Vac. Sci. Technol., A* **2012**, *30*, No. 021505.
(19) Chen, L.; Warburton, R. E.; Chen, K.-S.; Libera, J. A.; Johnson, C.; Yang, Z.; Hersam, M. C.; Greeley, J. P.; Elam, J. W. Mechanism for Al2O3 atomic layer deposition on LiMn2O4 from in situ measurements and ab Initio calculations. *Chem* **2018**, *4*, 2418−2435.
(20) Seo, S.; Yeo, B. C.; Han, S. S.; Yoon, C. M.; Yang, J. Y.; Yoon, J.; Yoo, C.; Kim, H.-J.; Lee, Y.-B.; Lee, S. J.; Myoung, J.-M.; Lee, H.-B.-R.; Kim, W.-H.; Oh, I.-K.; Kim, H. Reaction mechanism of area-selective atomic layer deposition for Al2O3 nanopatterns. *ACS Appl. Mater. Interfaces* **2017**, *9*, 41607−41617.
(21) Perdew, J. P.; Burke, K.; Ernzerhof, M. Generalized gradient approximation made simple. *Phys. Rev Lett.* **1996**, *77*, 3865−3868.
(22) Łodziana, Z.; Nørskov, J. K.; Stoltze, P. The stability of the hydroxylated (0001) surface of α-Al2O3. *J. Chem. Phys.* **2003**, *118*, 11179−11188.
(23) Elliott, S. D.; Greer, J. C. Simulating the atomic layer deposition of alumina from first principles. *J. Mater. Chem.* **2004**, *14*, 3246−3250.
(24) Hass, K. C.; Schneider, W. F.; Curioni, A.; Andreoni, W. First-principles molecular dynamics simulations of H2O on α-Al2O3(0001). *J. Phys Chem. B* **2000**, *104*, 5527−5540.
(25) Finger, L. W.; Hazen, R. M. Crystal structure and compression of ruby to 46 kbar. *J. Appl. Phys.* **1978**, *49*, 5823−5826.
(26) Nguyen, M.-T. Computational study of α-M2O3 (M = Al, Ga): surface properties, water adsorption and oxidation. *RSC Adv* **2015**, *5*, 38601−38609.
(27) Masango, S. S.; Hackler, R. A.; Henry, A.-I.; McAnally, M. O.; Schatz, G. C.; Stair, P. C.; Van Duyne, R. P. Probing the chemistry of alumina atomic layer deposition using operando surface-enhanced raman spectroscopy. *J. Phys. Chem. C* **2016**, *120*, 3822−3833.
(28) Goldstein, D. N.; McCormick, J. A.; George, S. M. Al2O3 atomic layer deposition with trimethylaluminum and ozone studied by in situ transmission FTIR spectroscopy and quadrupole mass spectrometry. *J. Phys. Chem. C* **2008**, *112*, 19530−19539.
(29) Ritala, M.; Juppo, M.; Kukli, K.; Rahtu, A.; Leskelä, M. In situ characterization of atomic layer deposition processes by a mass spectrometer. *J. Phys. IV France* **1999**, *09*, 1021−1028.

https://dx.doi.org/10.1021/acs.iecr.0c02382
Ind. Eng. Chem. Res. 2020, 59, 13325−13332

Supporting Information

Unveiled Understanding on Thermodynamic Mechanisms of Atomic Layer Deposition Based on Trimethylaluminum and Water Precursors

Jae Won Choi, So-Yeon Ham,§ Suhyun Lee, Da-Som Shin, Yo-Sep Min* and Ki Chul Kim*

Division of Chemical Engineering, Konkuk University, Seoul 05029, The Republic of Korea

Corresponding authors
*_Emails:_ ysmin@konkuk.ac.kr (Y. S. Min); kich2018@konkuk.ac.kr (K. C. Kim)
§Current affiliation: Department of Nano-Engineering, University of California San Diego

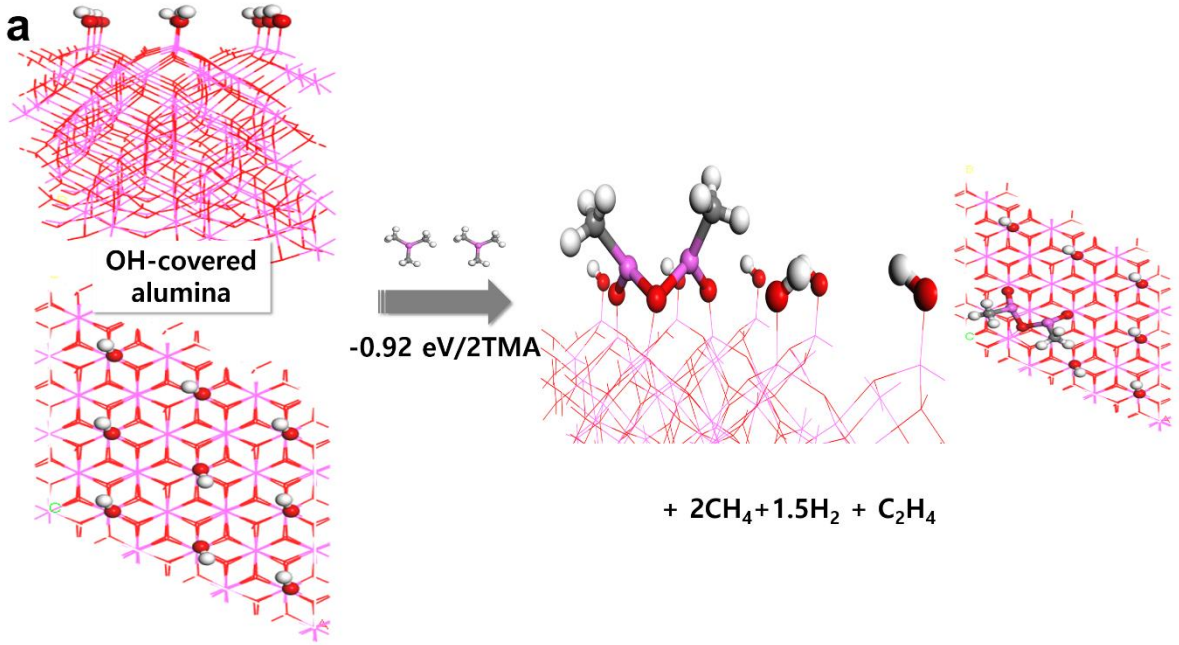
a
OH-covered
alumina
-0.92 eV/2TMA
+ 2CH4+1.5H2 + C2H4

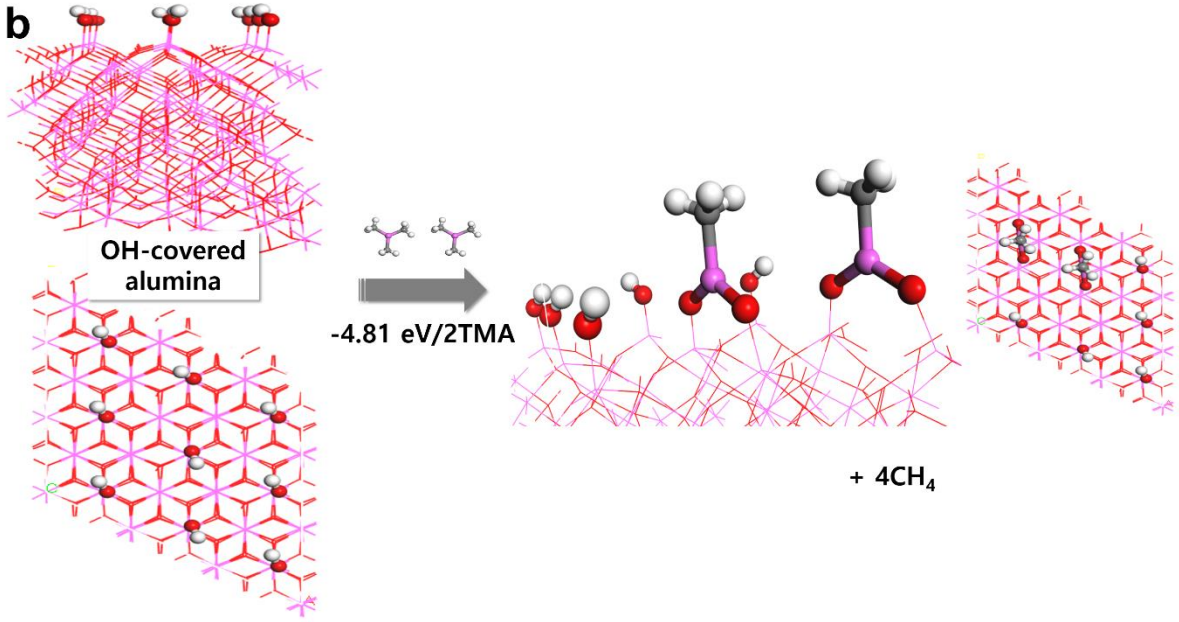
b
OH-covered
alumina
-4.81 eV/2TMA
+ 4CH4

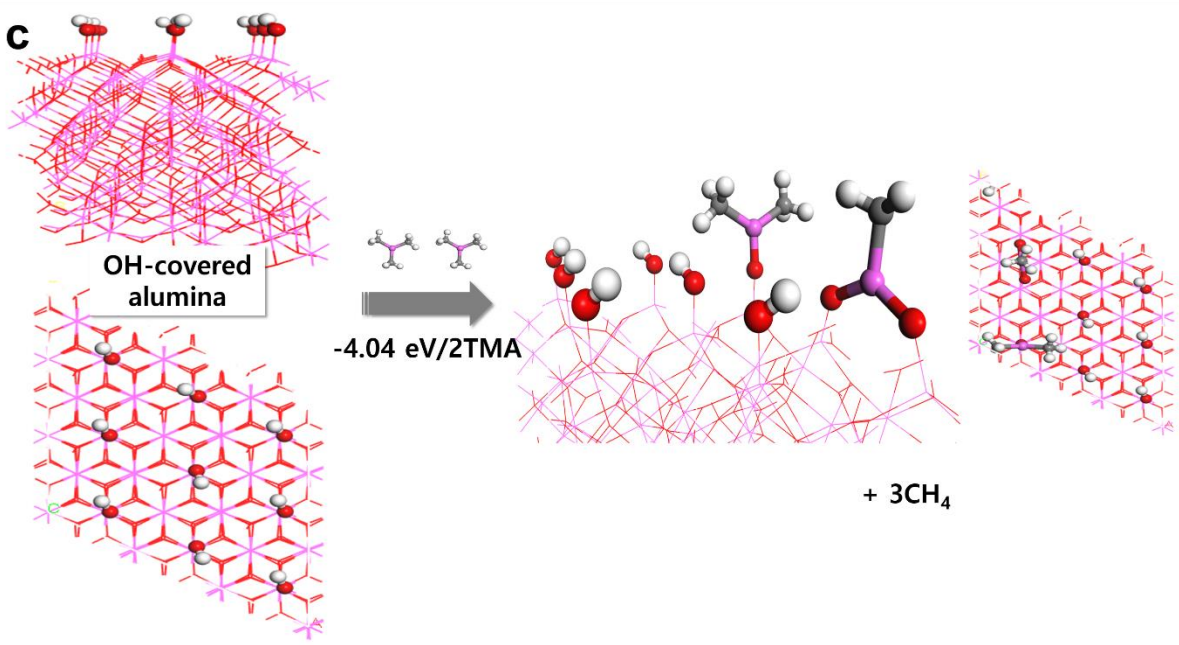
c
OH-covered
alumina
-4.04 eV/2TMA
+ 3CH4

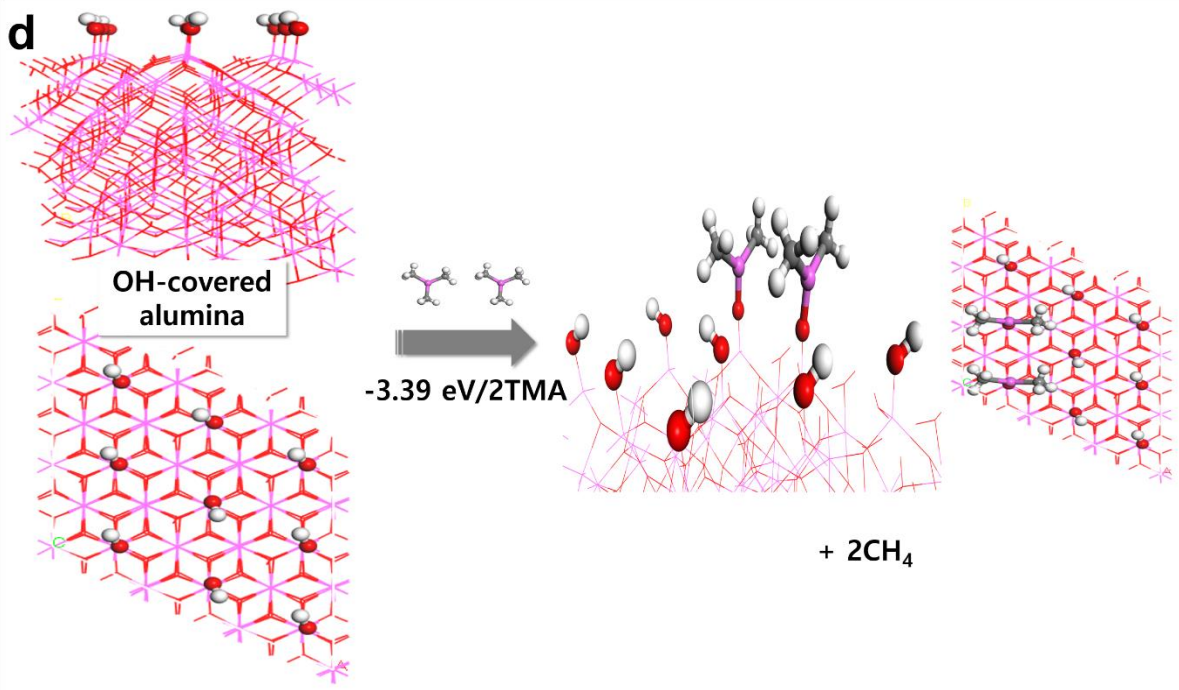
d
OH-covered
alumina
-3.39 eV/2TMA
+ 2CH4

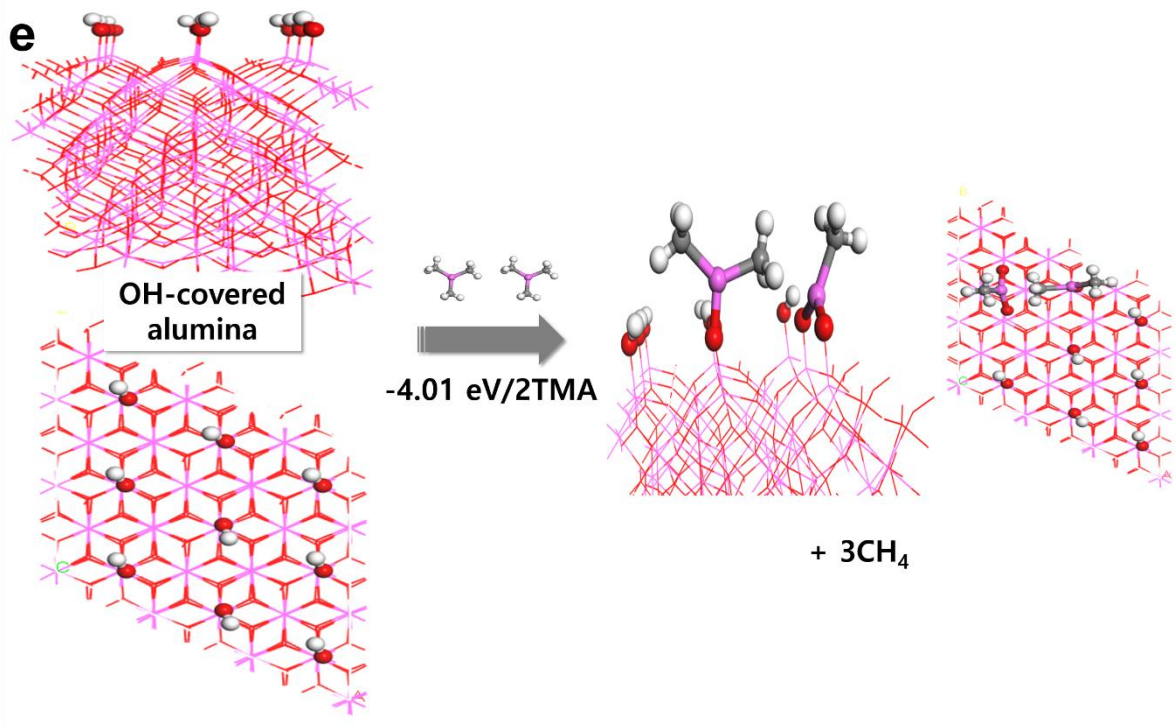

Figure S1. Reaction schemes for MS models. The visualization of the reaction schemes associated with the chemisorption of the five MS models, namely, (a) MS1, (b) MS2, (c) MS3, (d) MS4, and (e) MS5, on the hydroxylated Al_2O_3(0001) surfaces. The information on the formation energy in the unit of eV/2 TMA, and the byproducts (*i.e.*, CH_4, C_2H_4, or H_2) is also included in the schemes.

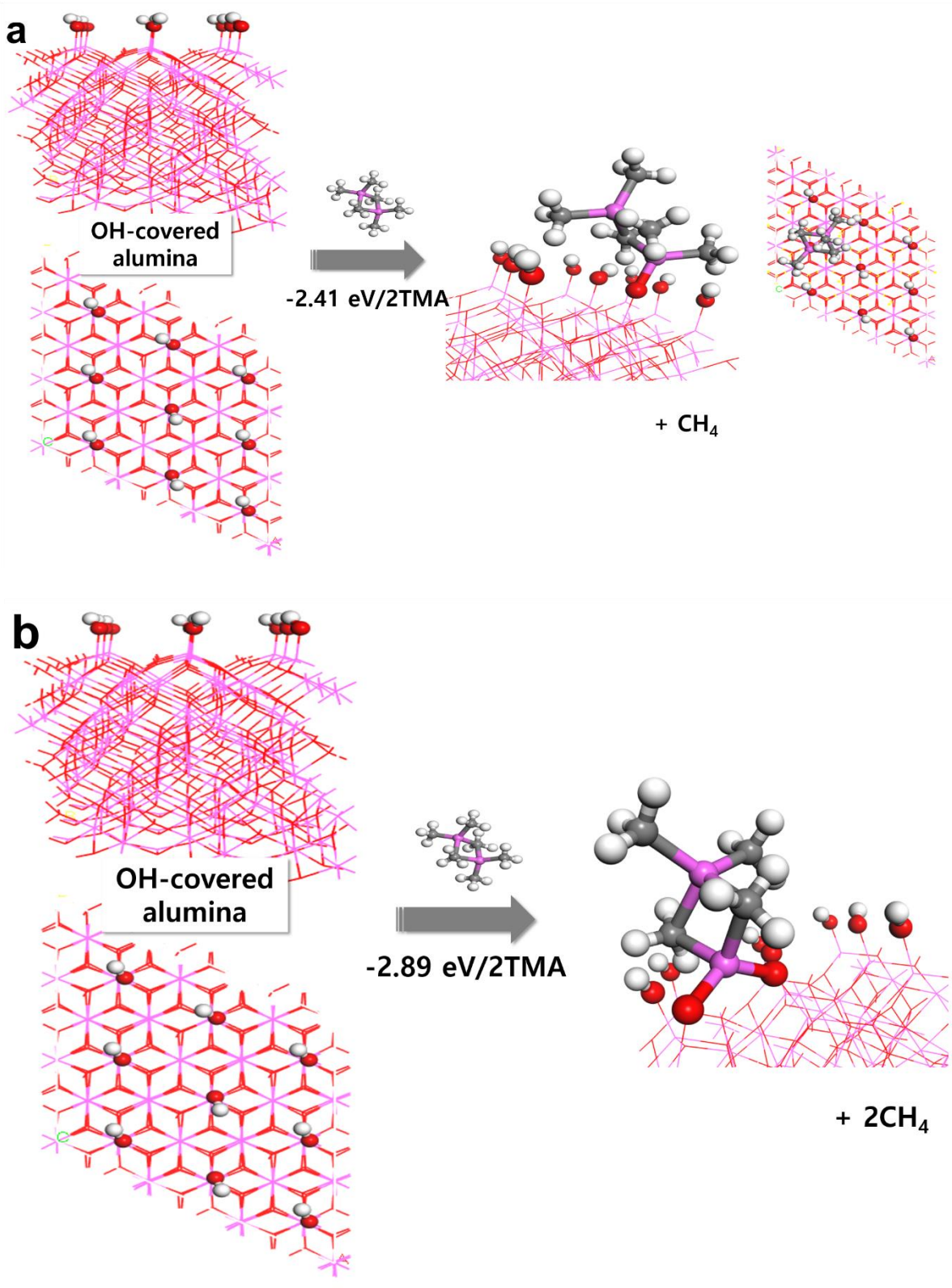

Figure S2. Reaction schemes for DS models. The visualization of the reaction schemes associated with the chemisorption of the two DS models, namely, (a) DS1 and (b) DS2, on the hydroxylated Al_2O_3(0001) surfaces. The information on the formation energy in the unit of eV/2 TMA, and the byproduct (*i.e.*, CH_4) is also included in the schemes.

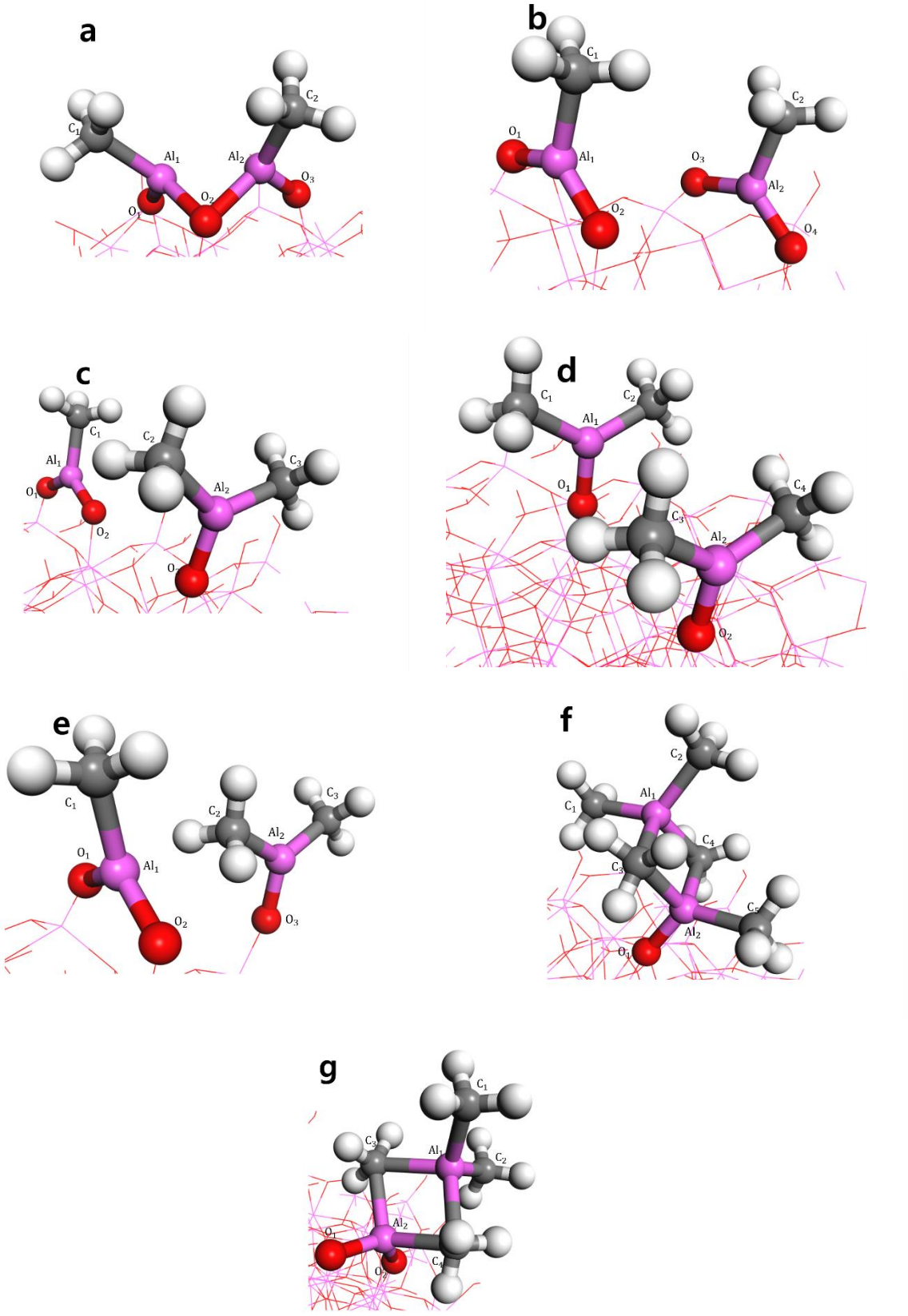

Figure S3. Labels for atoms in five MS and two DS models. The labels of surface TMA atoms for (a) MS1, (b) MS2, (c) MS3, (d) MS4, (e) MS5, (f) DS1, and (g) DS2 models.

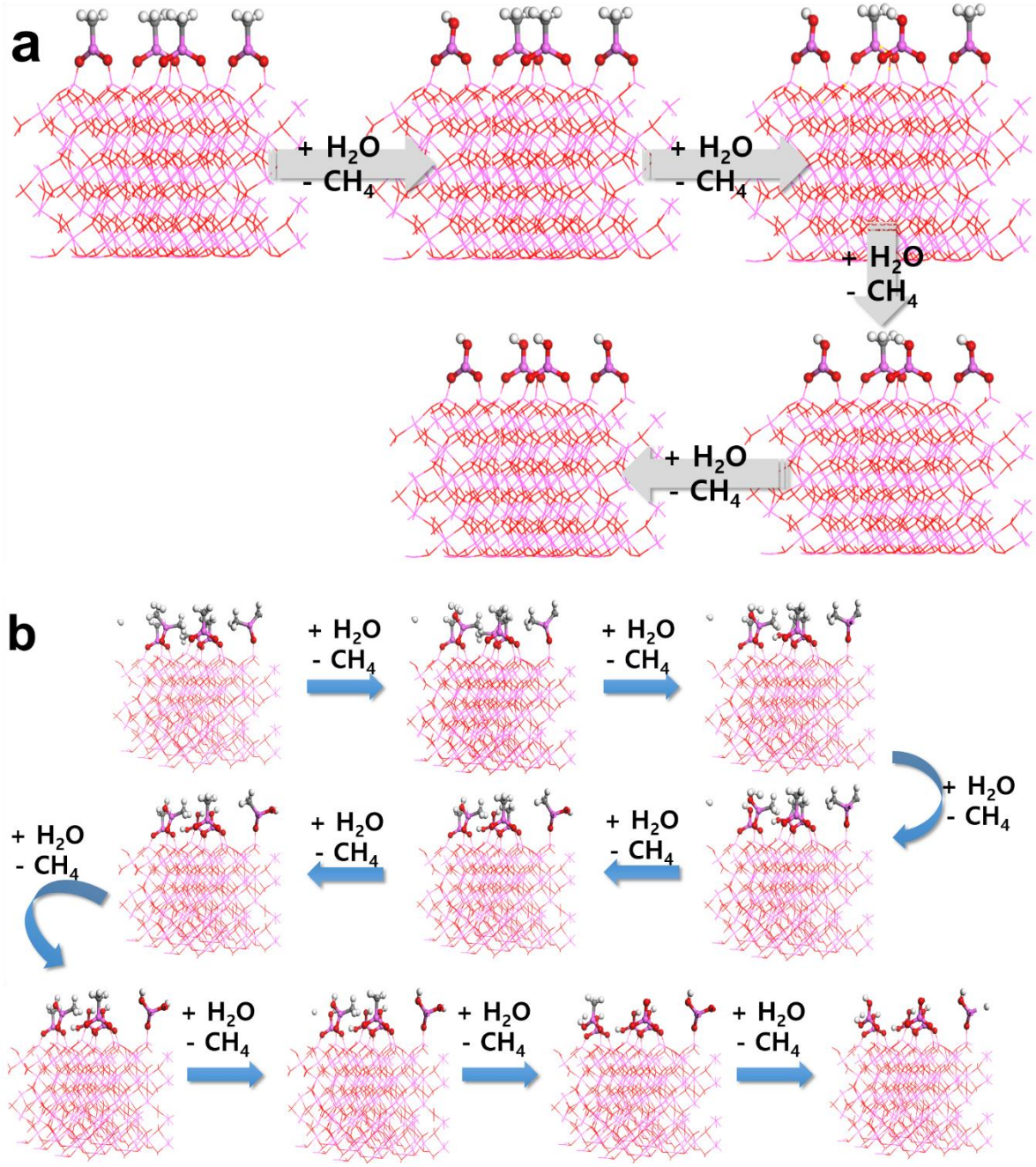

Figure S4. Reaction schemes for water chemisorption (side view). The side-viewed visualization of the reaction schemes associated with the chemisorption of water molecules on TMA-chemisorbed Al_2O_3(0001) surfaces for (a) MS2 and (b) MS3 configurations.

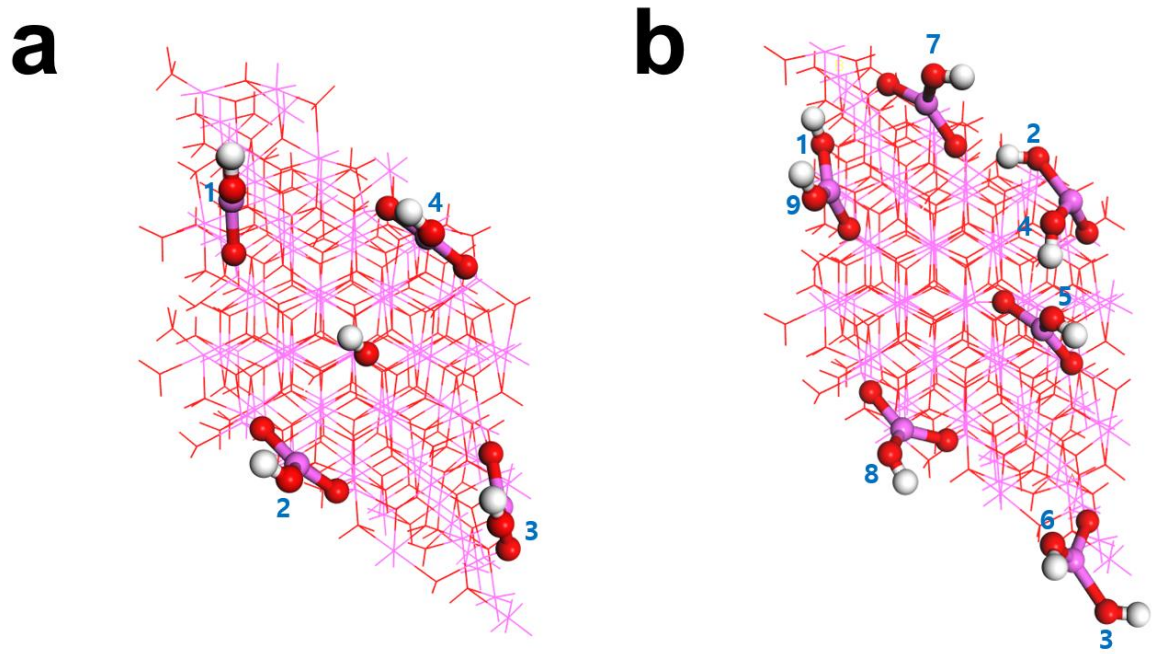

Figure S5. Reaction schemes for water chemisorption (top view). The top-viewed visualization of the reaction schemes associated with the chemisorption of water molecules on TMA-chemisorbed Al_2O_3(0001) surfaces for (a) MS2 and (b) MS3 configurations. The sequence of the hydroxyl groups generated as a result of the sequential chemisorption of water molecules is numbered in the figures.

Table S1. Information on the structural models. The structural information (*e.g.*, lattice parameters, bond length, and bond angle) on the bulk Al_2O_3 and its hydroxylated surface models developed in this study. The resultant values are compared with their theoretical/experimental values reported in previous studies.

Bulk Al_2O_3	Lattice parameter (Å)		
	a	b	c
This study	4.79	4.79	12.99
Elliott et al., *J. Mater. Chem.*, 14 (2004), 3246-3250	4.75	4.75	13.10
Finger et al., *J. Appl. Phys.*, 49 (1978), 5823-5826	4.76	4.76	12.99

Hydroxylated Al_2O_3 Surface	Bond angle (H-O-Al, °)
This study	115-123.5
Lodziana et al., *J. Chem. Phys.*, 118 (2003), 11179-11188	110-123.0

Hydroxylated Al_2O_3 Surface	Bond length (H-O, Å)
This study	0.97
Hass et al., *J. Phys. Chem. B*, 104 (2000), 5527-5540	0.97

Table S2. Formation energies in the unit of eV/2 TMA for seven models feasible from the TMA-based atomic layer deposition cycle.

Model	DS1	DS2	MS1	MS2	MS3	MS4	MS5
Formation energy in eV/2 TMA (kJ/mol of 2TMA)	-2.41 (-233)	-2.89 (-279)	-0.92 (-89)	-4.81 (-464)	-4.04 (-390)	-3.39 (-327)	-4.01 (-387)

Table S3. Change in the DFT-calculated sequential chemisorption energy during the water-based atomic layer deposition cycle for MS2 model.

No. of water molecules	1W	2W	3W	4W
Sequential chemisorption energy in unit of eV/H_2O (kJ/mol H2O)	-1.35 (-130)	-1.33 (-128)	-1.32 (-127)	-1.34 (-129)

Table S4. Change in the DFT-calculated sequential chemisorption energy during the water-based atomic layer deposition cycle for MS3 model.

No. of water molecules	1W	2W	3W	4W	5W	6W	7W	8W	9W
Sequential chemisorption energy in unit of eV/H_2O (kJ/mol H2O)	-1.48 (-143)	-2.15 (-207)	-2.99 (-289)	-1.49 (-144)	-1.51 (-146)	-1.37 (-132)	-1.76 (-170)	-1.59 (-153)	-1.43 (-138)